Angewandte Chemie
Eine Zeitschrift der Gesellschaft Deutscher Chemiker

Supporting Information

69451 Weinheim, Germany

Rapid High-Specificity microRNA Detection Using a Two-stage Isotachophoresis Assay**

*Giancarlo Garcia-Schwarz and Juan G. Santiago**

anie_201305875_sm_miscellaneous_information.pdf

SUPPORTING INFORMATION

S1. Reagents and materials

We purchased trizma base, 4-(2-Hydroxyethyl)piperazine-1-ethanesulfonic (HEPES), 3-(trimethoxysilyl)-propyl methacrylate, 40% acrylamide/bisacrylamide (29:1), and 70% perchloric acid from Sigma-Aldrich (St. Louis, MO). We purchased the photoinitiator 2,2-azobis[2-methyl-N-(2-hydroxyethyl) propionamide] (VA-086) from Wako Chemicals (Richmond, VA). We also purchased hydrochloric acid from J.T. Baker (Avantor Performance Materials, Center Valley, PA); and Tris-EDTA buffer and 30% hydrogen peroxide from EMD biosciences (Gibbstown, NJ). We purchased glacial acetic acid and sodium hydroxide from Mallinckrodt Chemicals (Avantor Performance Materials, Center Valley, PA). The DNase/RNase-Free distilled water and pre-mixed 1M Tris-HCl pH 8 was purchased from GIBCO (Carlsbad, CA). We purchased formamide from Promega (Madison, WI). We purchased the synthetic DNA and RNA oligonucleotides listed in **Table S1** from Genelink (Hawthorne, NY) and Integrated DNA Technologies (Coralville, IA). We stored reconstituted oligos in 10 mM Tris-HCl, and stored these oligo stock solutions at either -20°C or -80°C in 2–6 µl aliquots. The TaqMan MicroRNA Reverse Transcription Kit, Universal PCR Master Mix II (with UNG), and MicroRNA Assay were purchased from Life Technologies (Grand Island, NY). We performed quantitative RT-PCR with a MiniOpticon Real-Time PCR Detection System from Bio-Rad (Hercules, CA).

We purchased borosilicate glass microfluidic chips (model NS260) and separate plastic chip caddies from Caliper Life Sciences (Mountain View, CA). We attached chip caddies using ultra-violet (UV)-curing optical adhesive (NOA-68) purchased from Norland Products Inc. (Cranbury, NJ) and a UV lamp purchased from Zilla Products (Franklin, WI).

We performed UV-initiated polymerization of polyacrylamide hydrogels by filling chips with prepolymer solution and placing chips atop a 365 nm collimated LED lightsource (M365L2-C3) from Thorlabs (M365L2, Newton, NJ). We measured UV lightsource intensity (approximately 5 mW/cm^2 at the chip plane) using a digital UV light meter (UV513AB, General Tools, New York, NY).

S2. Experimental apparatus

All data were taken with a custom epifluorescent point-confocal microscopy setup, similar to that described previously.[1] Briefly, the setup consists of an inverted epifluorescent microscope (IX70, Olympus, Hauppauge, NY) with 40x water-immersion objective (LUMPlanFL, Olympus, Hauppauge, NY) and Cy5 filter cube (Cy5-4040A, Semrock, Rochester, NY). The microscope was outfitted with an XYZ automated stage (ASI, Eugene, OR). A 642 nm diode laser (Stradus-642, Vortran Laser Technologies, Sacramento, CA) was used for illumination and a photomultiplier tube (PMT) module (H6780-20, Hamamatsu Photonics, Japan) with data acquisition unit (C8908, Hamamatsu Photonics, Japan) for detection. The PMT was powered by a function generator (E3631A, Agilent Technologies, Santa Clara, CA) and operated at a rate of 66.7 Hz (15 ms sampling period with 10 ms integration time). We used a high-voltage sourcemeter (2410, Keithley Instruments, Cleveland, OH) to apply constant current to the microfluidic chip. We used a custom MATLAB (R2007b, Mathworks, Natick, MA) program to control the high voltage supply and PMT and to record data from both instruments.

S3. Preparation of prepolymer mastermix, ITP buffers, and surface modification reagents

We prepared two prepolymers, PP1 and PP2, to perform our assay. We prepared PP1 by combining urea (165 mg), water (115 µl), 1 M tris (100 µl), 1 M hydrochloric acid (50 µl), and 40% acrylamide/bisacrylamide (50 µl). We prepared PP2 by combining urea (165 mg), water (130 µl), 1 M tris (100 µl), 1 M hydrochloric acid (50 µl), 40% acrylamide (25 µl), and 5% w/w PVP (10 µl). We prepared the photoinitiator, VA-086, at a concentration of 2% (w/v), diluted in water. Using these

components and acrydite-modified oligos (capture probes) we prepared three distinct leading electrolyte (LE) prepolymer mixtures:

LE1: 135 µl PP1 + 15 µl VA-086

LE2: 135 µl PP2 + 15 µl VA-086

LE3: 38 µl LE1 + 2 µl capture probe

We found that fresh preparation of the prepolymers and photoinitiator before each use was important to assay repeatability. The photoinitiator (VA-086) is unstable under exposure to light and when dissolved in aqueous solution, and urea degrades significantly in aqueous solution at room temperature over the span of about one day.[2] The TE consisted of 10 mM HEPES, 20 mM Tris, and 50% formamide. Before each experiment, we combined 9 µl TE and 1 µl total RNA solution for a final RNA concentration of 100 ng/µl. We then heated this mixture in a thermal cycler 60°C for 10 min to disrupt secondary structure, and then immediately placed on ice. Finally, we added 1 µl of 5 nM hairpin reporter to this mixture (which we call TE+S) before using in our experiment.

S4. Microfluidic chip preparation, gel patterning, and *in situ* polymerization

We prepared a surface modification mixture consisting of 5:3:2 (v/v) DI water, acetic acid, and 3-(trimethoxysilyl)-propyl methacrylate, used to modify channel surface properties and promote covalent attachment of hydrogel to the glass surface. We followed the same chip preparation protocol as reported previously,[1] with minor modifications:

1. Rinse with DI water for 5 min
2. Rinse with 1 M sodium hydroxide for 5 min
3. Rinse with DI water for 1 min
4. Empty reservoirs and apply vacuum to dry for 1 min
5. Rinse with surface modification mixture for 5 min
6. Rinse with 30% acetic acid for 1 min
7. Rinse with DI water 5 min
8. Empty reservoirs and apply vacuum to dry for 1 min

We then filled the chip with the three prepolymer solutions, as shown in the chip layout schematic of **Fig. S1**. We filled reservoirs 1 through 4 with 10 µl LE1 each, reservoirs 5 and 6 with 10 µl LE2 each, and reservoirs 7 and 8 with 10 µl LE3 each. We then applied vacuum to the microfluidic chip at reservoirs 4 and 6 for approximately 1.5 min. We then carefully removed both vacuum lines simultaneously and transferred the chip to our UV LED light source (with ~5 mW/cm^2 intensity) for 10 min to form the LPA and PA polymers. Following UV exposure, we flushed away unattached oligos from the LE3 region channel by applying 2 µA current between reservoirs 5 and 8 for 5 min.

S5. Protocol for experiments in this paper

We performed our assay immediately following chip preparation (described in the previous section). Our assay operation consisted of three stages: semi-infinite sample injection, hybridization, and detection. We carried out these stages according to the sourcemeter protocol summarized in **Table S2**. This procedure resulted in a type of "finite sample injection" strategy, which we used to avoid any increase in background signal during the capture phase of the experiment. In previous work, we found that this injection mode resulted in larger enhancement ratios and therefore improved sensitivity and dynamic

range (compared to a semi-infinite injection scheme where we continuously draw target from the same TE reservoir).[1]

In the injection stage, we performed a semi-infinite injection from the TE+S reservoir (reservoir 1 in **Fig. S1**), where sample was continuously injected from the input reservoir. We stopped the combined sample and reporter injection process at approximately $t = 450$ s when the ITP zone reached detection station 0 (DS0), as shown in the chip schematic of **Fig. S1** (depicted by the first dashed vertical line in **Fig. 2** of the main text). For the hybridization stage, we switched the source of TE anions to a secondary TE reservoir (reservoir 5 in **Fig. S1**) containing only TE (without target or reporter molecules). We performed our first critical fluorescence measurement at DS1, just before the start of the purification region (LE3), as an internal normalization control. Finally, we allowed the ITP zone to enter the purification region, where we performed two additional fluorescence measurements at locations DS2 and DS3, respectively 0.9 cm and 1.9 cm after the start of the capture gel.

S6. Data analysis and let-7a quantification

The key signals (integral of PMT signal vs. time) measured in each experiment were:

- Normalization peak (N): integrated peak measured at location DS1, downstream of the capture gel
- Signal peaks (D): integrated peak measured at locations DS2 and DS3, upstream of the capture gel

Peak integration consisted of fitting a Gaussian to the PMT signal vs. time, and then integrating the fitted Gaussian curve to quantify signal intensity, as described previously.[1] For this analysis we assumed that the velocity of the ITP zone is the same for each experiment. This assumption is reasonable when chip-to-chip variations in geometry are minimal, and assuming we apply the same constant current conditions in each experiment, as the ITP velocity scales with the electric field.

We then calculated the final measured signal for each experiment using the following equation:

$$S_i = \frac{D_i - B}{N_i - B}.$$

Here S_i is the measured signal for experiment i, and B is the background signal, defined as the integrated peak intensity at location DS3 for a negative control experiment. We found that B did not vary with changes in the normalization peak for negative control experiments.

For let-7a quantification experiments shown in **Fig. 4** of the main text, we constructed a simple calibration curve, shown in **Fig. S2**. We performed spike-in experiments for let-7a concentrations of 0, 50, 150, and 500 pM, which spanned the concentrations of let-7a in 100 ng/µl total RNA of the samples measured. We obtained three measurements for the negative control (0 pM let-7a), which we averaged, and one measurement each for the other concentrations. For these experiments we included total RNA from K562 cells (which does not contain let-7a, as verified by qPCR) to increase background RNA complexity. We performed a linear least squares fit to calibration curve data with zero intercept, which we then used to determine absolute concentrations of let-7a from experiments with total RNA purified from tissues and cell culture.

S7. Gel patterning and preventing gel degradation

We observed bubble formation and severe and observable degradation of the gel in our experiments when injecting long DNA or RNA directly from free solution into LE2 (4% PA). As an example of this phenomenon, **Fig. S3** shows the effect of focusing 70 nt and 200 nt DNA with ITP and electromigrating

from free solution into a 4% PA gel. These experiments focused initial concentrations of approximately 1 μM. While 70 nt DNA enters the gel without any visible disruption, 200nt DNA appears to immediately deflect the gel boundary and eventually causes bubbles to form along the center axis of the channel (i.e., visible signal depletion along the channel centerline). The gel appears to "tear" along a region near the center of the channel when injecting high concentrations of long nucleic acids. We did not observe this effect at significantly lower concentrations of 200 nt DNA (data not shown). We observed similar behavior when injecting total RNA. Above a threshold concentration of ~20 ng/μl, injecting total RNA caused bubble formation which resulted in voltage fluctuations in our experiments (see **Fig. S4a**).

A similar type of severe gel degradation was also reported by the group of Norman Dovichi in their work on Sanger sequencing capillary electrophoresis separations.[3] They observed bubble formation and large voltage fluctuations in their experiments, and identified high NA concentration as one of several common causes of gel degradation. In their experiments, increases in NA length and/or concentration were also associated with greater likelihood of gel degradation. We therefore hypothesized that sieving high concentration large RNAs (e.g., mRNA and rRNA molecules) out of the ITP zone prior to entering LE2 would eliminate gel degradation. We previously used a linear polymer to exclude long RNAs from the focused ITP zone;[4] here we used a low concentration linear polymer (LE1, composed of 2% linear polyacrylamide). We found that this matrix did not degrade even at a total RNA concentration of 100 ng/μl, as shown in **Fig. S4a** (red dash-dotted). Importantly, the use of LE1 for RNA injection prevented downstream degradation at the transition from LE1 to LE2 (see **Fig. S4b**).

We note that it is possible to use 2% LPA in all assay regions (injection, hybridization, and purification) rather than switch between 2% LPA and 4% PA. However, we opted to use 4% PA in the purification region (LE3) because studies by Rubina *et al.*[5] and Chan and Krull[6] suggest that incorporation of Acrydite-labeled oligos into the hydrogel matrix depends strongly on polymer precursor concentration. By using a higher concentration polymer, we aimed to enhance capture efficiency and therefore improve sensitivity and dynamic range of our assay. We used 4% PA in the hybridization region (LE2) primarily for consistency between the normalization and final detection signals (measured at locations DS0 and DS2, respectively, in **Fig. S1**). In addition, we note that 4% PA performs some size-selection. As seen in **Fig. S3**, DNA of length ~200 nt and above will not focus in regions with 4% PA. Size selection greatly reduces sample complexity can improve specificity.[7]

S8. Simulation of assay hybridization dynamics using a volume-averaged model

We simulated hybridization dynamics of our assay using a volume-averaged model adapted from Bercovici *et al.*[8] The second-order reaction dybnamics in terms of volume-averaged concentration values are described by:

$$\frac{dc_T}{dt} = -\frac{3}{\sqrt{\pi}} k_{on} c_T c_R + k_{off} c_H + F(t) c_T^0$$

$$\frac{dc_R}{dt} = -\frac{3}{\sqrt{\pi}} k_{on} c_T c_R + k_{off} c_H + F(t) c_R^0$$

$$\frac{dc_H}{dt} = \frac{3}{\sqrt{\pi}} k_{on} c_T c_R - k_{off} c_H \, .$$

Here c_T, c_R, and c_H are the volume-averaged target, reporter, and hybrid concentrations, c_T^0 and c_R^0 are the target and reporter concentrations in the TE, and k_{on} and k_{off} are the on- and off-rate constants,

respectively. The function $F(t)$ represents the accumulation rate during sample and reporter injection, defined as:

$$F(t) = \begin{cases} F_0 & t < t_{inj} \\ 0 & t \geq t_{inj} \end{cases},$$

where t_{inj} is the total injection time.

We use these equations to model sample injection and hybridization during the first stage of the assay, for $t < t_{inj} + t_{hyb}$, where t_{hyb} is the post-injection hybridization time (see **Section S5** for assay protocol). In the second stage, the ITP zone migrates through a gel decorated with capture probes which removes reporters from the ITP reaction volume. We assume that binding between reporters and capture probes occurs on a much faster timescale than melting of reporters from target molecules, i.e., $k_{on,P} c_P \gg k_{off}$ where $k_{on,P}$ is the on-rate for the reporter-capture probe reaction and c_P is the effective concentration of capture probes. We believe this is a good assumption because capture probes contain 50% LNA composition, which significantly increases their affinity for reporters. In addition, we estimate the concentration of capture probes is on the same order as reporters focused in the ITP zone, i.e., $c_P \geq c_R$,[1] which suggests the capture gel has sufficient capacity to remove excess reporters immediately upon entry of the ITP zone. Based on these estimates and assumptions, we set $c_R = 0$ in the purification stage (for $t \geq t_{inj} + t_{hyb}$).

We use a combination of experimental measurements and simulations to determine kinetic rate constants. For all sequences, we determined k_{off} experimentally (see **Section S9**, below). For let-7a, we used K_D as a fitting parameter to determine a best fit to our titration data (see **Fig. 3b** inset in the main text). We then used the equilibrium relation, $K_D = k_{off}/k_{on}$, to determine k_{on}. Additionally, we used the DINAMelt web server to calculate K_D as a function of temperature for let-7a and all mismatches using the relation $K_D(T) = c_T(T)c_R(T)/c_H(T)$.[9] This allowed us to compare K_D across all sequences for any fixed value of T. Because we used denaturant and not temperature to optimize assay stringency, we determined an "effective temperature", T_{eff}, by evaluating the relation above for $K_D(T)$ using the fitted K_D for let-7a. We found $T_{eff} = 51°C$. We then used this T_{eff} to evaluate the appropriate values of K_D for each reporter-mismatch reaction (using the respective $K_D(T)$ curve for each reporter-mismatch pair).

Importantly, we consider these estimates and this model as only a semi-quantitative estimate of the dynamics of the respective species concentrations. The main utility of this model is estimating the trade-off between signal strength and stringency. For example, placing the detector further downstream of the start of the capture gel results in increase in stringency but lower signal. This tradeoff is well-demonstrated by **Fig. 2b** in the main text. We note this model is not required to create a calibration curve, which we use to establish a quantitative relationship between measured raw signals and target molecule concentration.

S9. Estimation of kinetic off-rates

In the purification stage of our assay, the absence of free reporters (assuming they are removed rapidly by the capture gel, as described in **Section S8**) results in the following reaction equation:

$$\frac{dc_H}{dt} = -k_{off} c_H .$$

Given this approximate relation, we can estimate the off-rate for a given sequence by simply measuring peak signal at two locations (c_1 and c_2) in the purification region. We use these measurements and the time elapsed between them, Δt, to estimate:

$$k_{off} = -\frac{1}{c_H}\frac{dc_H}{dt} \approx \frac{2}{\Delta t}\left(\frac{c_1 - c_2}{c_2 + c_1}\right).$$

We perform these two measurements in our assay at locations DS2 and DS3 as described in **Section S5** and shown in **Fig. S1**. In **Fig. S5** we plot the k_{off} values of let-7c, 7d, and 7e mismatches relative to that of let-7a. We note that all mismatch k_{off} values are greater than that of let-7a. This demonstrates that the combined effect of thermodynamics and kinetics results in the excellent stringency demonstrated here. Our two-step approach therefore takes advantage of off-rate kinetics to improve specificity. This is in contrast to one-step assays, which do not perform reaction purification (e.g., molecular beacons).

S10. Hairpin reporters do not hybridize to precursor microRNA molecules

Precursor microRNAs are ~80nt long molecules that share the mature microRNA sequence, but are inactive and hence typically must be excluded from the quantitative measurement of the mature microRNA of interest.[10] This poses a challenge for hybridization methods which rely on complementary hybridization probes that can bind to both mature and precursor microRNAs. In a previous publication, we used linear reporter molecules and demonstrated selectivity for let-7a over the let-7a precursor (pre-let-7a) by using a secondary affinity capture gel to remove precursors.[1] We achieved this by designing capture probes complementary to the pre-let-7a "loop" region, which is not present in the mature form.

In this work, we found that simply using hairpin-shaped reporters conferred this selectivity without the need for a secondary capture region (see **Fig. 2c** in the main manuscript). We note that both the hairpin reporter and pre-let-7a have strong secondary structures which introduce competition between folding and hybridization. To demonstrate the effect of this competition on hybridization, we numerically generated melting curves for pre-let-7a and three reporter designs using the DINAMelt web server,[9] as shown in **Fig. S6**. We note that a linear reporter will hybridize quite well with pre-let-7a at room temperature. However, a hairpin design with 6 nt stem reduces the equilibrium fraction dramatically, and a hairpin design with 8 nt stem (used in our experiments) completely eliminates hybridization to pre-let-7a. We hypothesize that this approach is generally applicable, as all precursor microRNAs have a distinct hairpin structure.

When designing a hairpin reporter against a new microRNA, we recommend first optimizing stem length and GC content numerically (using DINAMelt simulations) until $\Delta T \approx 5°C$ between target and mismatches. We then recommend optimizing stem length and GC content further, if needed and again using DINAMelt simulations, to ensure the hairpin reporter will not hybridize to the precursor molecule corresponding to the target microRNA. In both optimizations, increasing stem length or GC content will improve discrimination between target, precursor, and mismatches.

S11. Estimate of amount of RNA processed by ITP

We here preset an estimate of the amount of RNA which we process using our off-the-shelf chip and simple injection protocol. The amount of RNA processed by our ITP assay is influenced by three factors: analyte mobility relative to the TE ion mobility, adjusted TE ion concentration (i.e., the concentration of TE ions in the regions formerly occupied by the LE), and time allowed for RNA injection. The analyte travels at velocity U_A through a channel with cross-sectional area A, for total injection time T. The flux of analyte of concentration, c_A, in the frame of reference of the moving ITP interface, U_{ITP}, is

$$Q_A = c_A\left(U_A - U_{ITP}\right)A.$$

Expressed in terms of ion electrophoretic mobilities we find

$$Q_A = c_A\left(\frac{\mu_A}{\mu_{TE}} - 1\right)U_{ITP}A\,.$$

To find the total mass accumulated, we simply multiply by the total time over which the analyte injection occurs,

$$M_{inj} = c_A\left(\frac{\mu_A}{\mu_{TE}} - 1\right)U_{ITP}AT\,.$$

We note that the ITP velocity multiplied by the injection time is equal to the channel length over which the ITP interface travels, *L*, which is fixed by the detection point location (DS0 in **Fig. S1**) in our experiments, therefore

$$M_{inj} = c_A\left(\frac{\mu_A}{\mu_{TE}} - 1\right)AL\,.$$

In addition, the Jovin and Alberty regulating functions set by the LE buffer which initially fills the channel causes the TE ions (and all analytes mixed in the TE) to adjust to a new concentration as it enters the channel.[11] For our experiments, we estimate a 5-fold change in concentration between the analyte concentration dispensed in the reservoir and that which enters the channel, $c_A \approx 5c_{A,res}$. We also estimate an analyte-to-TE ion mobility ratio of $\mu_A/\mu_{TE}\approx 1.5$. With these estimates, we find:

$$M_{inj} = 2.5c_{A,res}AL\,.$$

The fraction analyte injected from the TE reservoir is then simply the ratio of mass accumulated in the ITP zone (M_{inj}) to that dispensed in the TE reservoir (M_{res}):

$$f = \frac{M_{inj}}{M_{res}} \approx \frac{2.5c_{A,res}AL}{c_{A,res}V} = \frac{2.5AL}{V}\,.$$

So we find that the fraction injected is proportional to the volume swept by the ITP interface, *AL*, divided by the volume dispensed in the reservoir, *V*.

For the dimensions of the microfluidic chips used in our experiments, we find $f \approx 0.5\%$. Therefore, while we typically dispense 1 μg of total RNA in the chip reservoir, only ~5 ng of this enters the channel and focuses at the ITP interface. We note that this fraction of processed sample can be drastically increased with alternate chip configurations and injection protocols.

S12. Effect of magnesium on assay sensitivity and stringency

Magnesium is a divalent cation which enhances kinetic on-rates for DNA and RNA hybridization. We experimentally measured the effect of magnesium on sensitivity and stringency of our ITP assay. We performed experiments using our optimized leading buffer (LE) and the same buffer but with added 1 mM magnesium chloride (LE'). In **Fig. S7a** we show measurements of spike-in experiments using let-7a (target), let-7c (1nt mismatch), and let-7f (1nt mismatch). Magnesium increased let-7a signal by ~41%. While this signal increase can potentially improve sensitivity, it is acompanied by a decrease in specificity: we see that relative let-7c signal increases from 10% to 38%, and the relative let-7f signal increases from 0% to 21%. We also performed negative control experiments using both LE and LE' buffers (**Fig. S7b**) which we used to quantify background signal and efficiency of the capture-based

purification process. We note that magnesium improves capture efficiency by about 2-fold, which has direct implications for assay sensitivity and dynamic range.[1] Using the LE' buffer, we estimate the combined improvements in assay signal and background signal would result in ~3 pM sensitivity and 300-fold dynamic range (but, again, this would come at the cost of a reduction in specificity).

References

[1] G. Garcia-Schwarz, J. G. Santiago, *Anal. Chem.* **2012**, *84*, 6366-6369.

[2] M. He, A. E. Herr, *Nat. Protoc.* **2010**, *5*, 1844-1856; H. L. Welles, A. R. Giaquinto, R. E. Lindstrom, *J. Pharm. Sci.* **1971**, *60*, 1212-1216.

[3] D. Figeys, N. J. Dovichi, *J. Chromatogr. A* **1993**, *645*, 311-317; H. Swerdlow, K. E. Dew-Jager, K. Brady, R. Grey, N. J. Dovichi, R. Gesteland, *Electrophoresis* **1992**, *13*, 475-483.

[4] A. Persat, R. R. Chivukula, J. T. Mendell, J. G. Santiago, *Anal. Chem.* **2010**, *82*, 9631-9635; A. Persat, J. G. Santiago, *Anal. Chem.* **2011**, *83*, 2310-2316.

[5] A. Y. Rubina, S. V. Pan'kov, E. I. Dementieva, D. N. Pen'kov, A. V. Butygin, V. A. Vasiliskov, A. V. Chudinov, A. L. Mikheikin, V. M. Mikhailovich, A. D. Mirzabekov, *Anal. Biochem.* **2004**, *325*, 92-106.

[6] A. Chan, U. J. Krull, *Anal. Chim. Acta* **2006**, *578*, 31-42.

[7] M. Baker, *Nat. Methods* **2010**, *7*, 687-692.

[8] M. Bercovici, C. M. Han, J. C. Liao, J. G. Santiago, *Proc. Natl. Acad. Sci.* **2012**, *109*, 11127-11132.

[9] N. R. Markham, M. Zuker, *Nucleic Acids Res.* **2005**, *33*, W577-W581.

[10] K. A. Cissell, S. Shrestha, S. K. Deo, *Anal. Chem.* **2007**, *79*, 4754-4761.

[11] B. Jung, R. Bharadwaj, J. G. Santiago, *Anal. Chem.* **2006**, *78*, 2319-2327; R. A. Alberty, *J. Am. Chem. Soc.* **1950**, *72*, 2361-2367; T. M. Jovin, *Biochemistry* **1973**, *12*, 871-879.

Table S1. Synthetic oligonucleotide sequences and associated purification methods. Purification methods included high pressure liquid chromatography (HPLC) and polyacrylamide gel electrophoresis (PAGE).

Name	Type	Sequence	Purification method
let-7a	RNA	5-UGA GGU AGU AGG UUG UAU AGU U	PAGE
pre-let-7a	RNA	5-UGG GAU GAG GUA GUA GGU UGU AUA GUU UUA GGG UCA CAC CCA CCA CUG GGA GAU AAC UAU ACA AUC UAC UGU CUU UCC UA	PAGE
let-7b	RNA	5-UGA GGU AGU AGG UUG UGU GGU U	PAGE
let-7c	RNA	5-UGA GGU AGU AGG UUG UAU GGU U	PAGE
let-7d	RNA	5-CGA GGU AGU AGG UUG CAU AGU U	PAGE
let-7e	RNA	5-UGA GGU AGG AGG UUG UAU AGU U	PAGE
let-7f	RNA	5-UGA GGU AGU AGA UUG UAU AGU U	PAGE
let-7g	RNA	5-UGA GGU AGU AGU UUG UAC AGU U	PAGE
let-7i	RNA	5-UGA GGU AGU AGU UUG UGC UGU U	PAGE
capture probe	DNA/ LNA	5-/Acr/ +TG+A G+GT +AG+T A+GG +TT+G T+AT +AG+T T	HPLC
hairpin reporter	DNA	5-/Cy5/ CGC CGA GCA ACT ATA CAA CCT ACT ACC TCA GCT CGG CG	PAGE

*In the capture probe sequence, bases with an LNA sugar are preceded by "+".
**In the hairpin reporter sequence, we underline the portion complementary to let-7a and capture probe.

Table S2. Sourcemeter current program. We applied 1 μA constant current between ground (GND) and positive (HI) electrodes. A dash "-" under the reservoir listing indicates a floating voltage potential.

Name	Duration (approx.) [s]	Laser power [mW]	Reservoir #							
			1	2	3	4	5	6	7	8
Injection	450	1	GND	-	-	-	-	-	-	HI
Detection	300	1 to 5	-	-	-	-	GND	-	-	HI

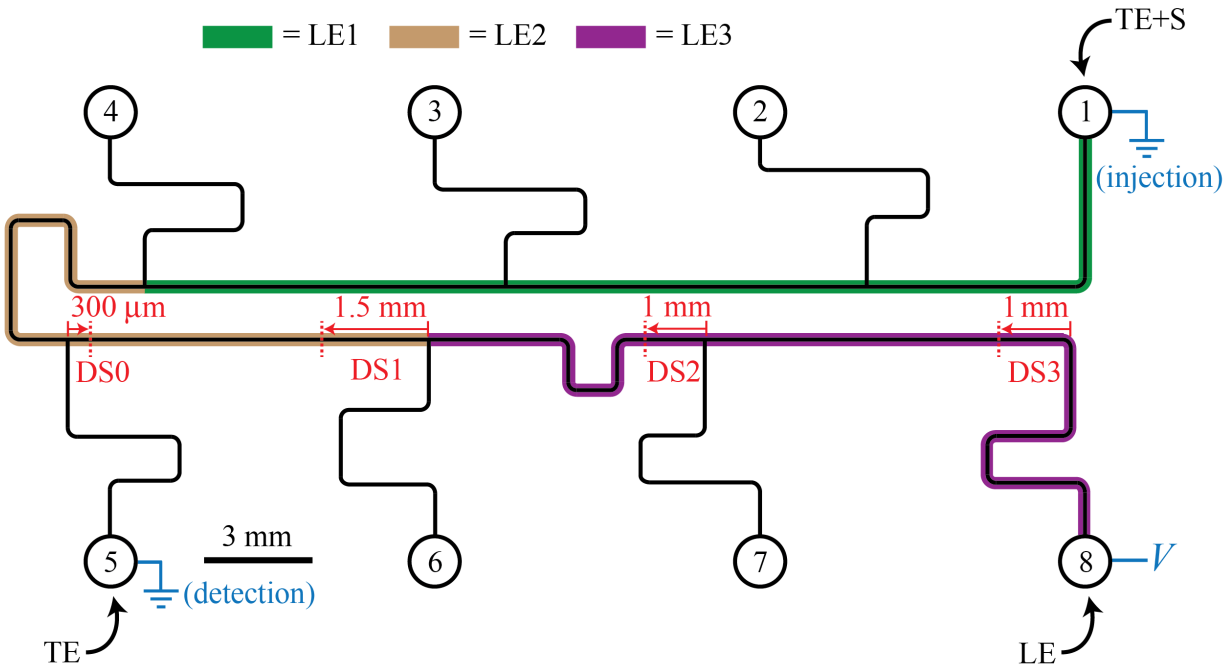

Figure S1. Caliper model NS260 microfluidic chip layout and indication of dispensed solutions (black), voltage program (blue), detection stations (red), and hydrogel patterning (green, brown, and purple). TE+S, TE, and LE were all dispensed prior to initiation of the voltage program. We apply the voltage program shown in **Table S2**. We first detect the ITP peak at detection station 0 (DS0). Once the peak passed DS0, we wait 3 s before we turn off the voltage supply and switch the ground electrode from reservoir 1 (TE+S) to reservoir 5, which contains clean TE. We then moved the detector to DS1 and resume the voltage program. We note that this manual step can be automated using an off chip voltage sequencer. We then detect the ITP peak at DS1, 1.5 mm before the start of the capture gel, as an internal normalization control. Finally, we detect the ITP peak at DS2 and DS3, respectively 0.9 mm and 1.9 mm after the start of the capture gel. Of these post-purification measurements, we use only the measurement at DS3 for specificity experiments (**Fig. 3** in the main text) and real sample experiments (**Fig. 4** in main text). We use both DS2 and DS3 measurements to estimate kinetic off-rates for let-7a and mismatches (see **Fig. S5**).

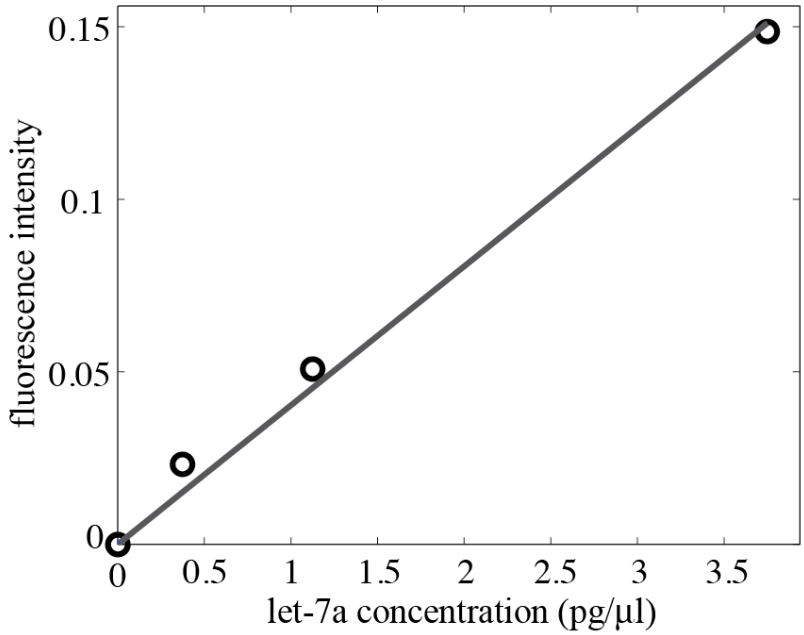

Figure S2. Calibration curve used for quantification of let-7a in total RNA extracts. We performed spike-in experiments for let-7a concentrations of 0, 50, 150, and 500 pM, which spanned the concentrations of let-7a in 100 ng/µl total RNA of the samples measured in **Fig. 4** of the main manuscript. In these experiments, we included 100 ng/µl total RNA from K562 cells to simulate background complexity of a real RNA sample.

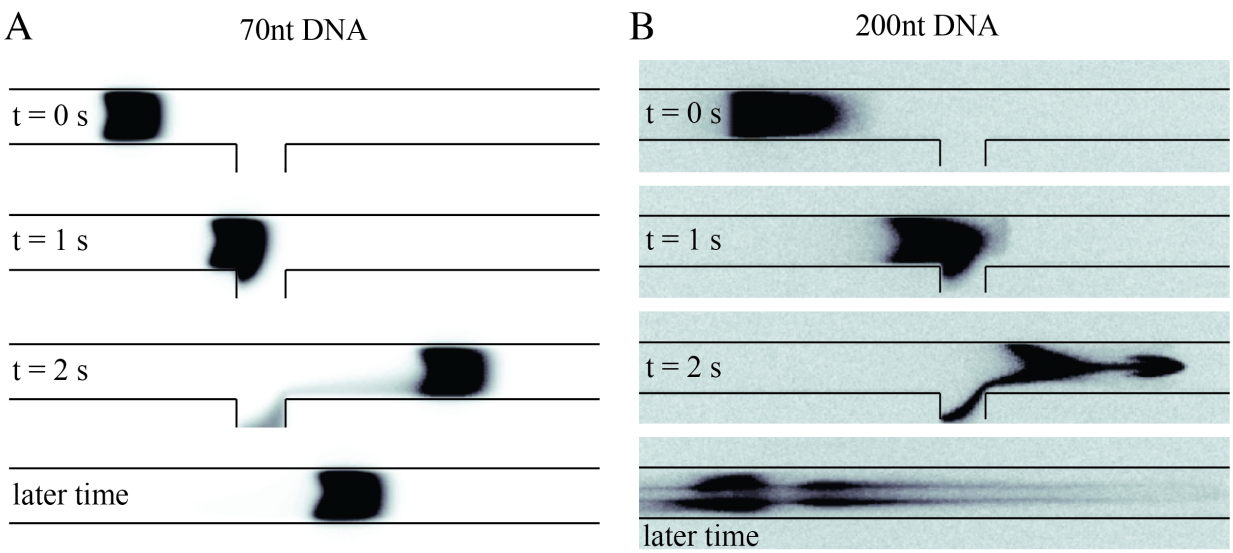

Figure S3. Experimental observation of gel degradation caused by high concentration long nucleic acids. We used ITP to focus 70nt and 200nt DNA in free solution, and allowed the focused nucleic acids to migrate into a region of the channel containing 4% crosslinked polyacrylamide. We patterned the hydrogel hydrodynamically, by applying vacuum at the side channel (shown in the top three images) to fill the left portion with pure LE buffer and the right portion with LE buffer containing gel precursor and photoinitiator. We then performed ITP focusing and used an intercalating dye to visualize the DNA. (A) The 70nt DNA crosses the free solution-gel interface without causing any disruptions (first three time-course images). We observed at a later time that the 70nt DNA remains focused in the hydrogel region downstream. (B) The 200nt focuses in free solution, but upon crossing the hydrogel interface appears to concentrate near the channel center. Observation of the DNA at a later time reveals a depleted signal in the channel center, which suggests bubble formation. We note that the 200nt DNA does not remain focused in ITP within the hydrogel region, as demonstrated by its increased diffusion along the channel axis.

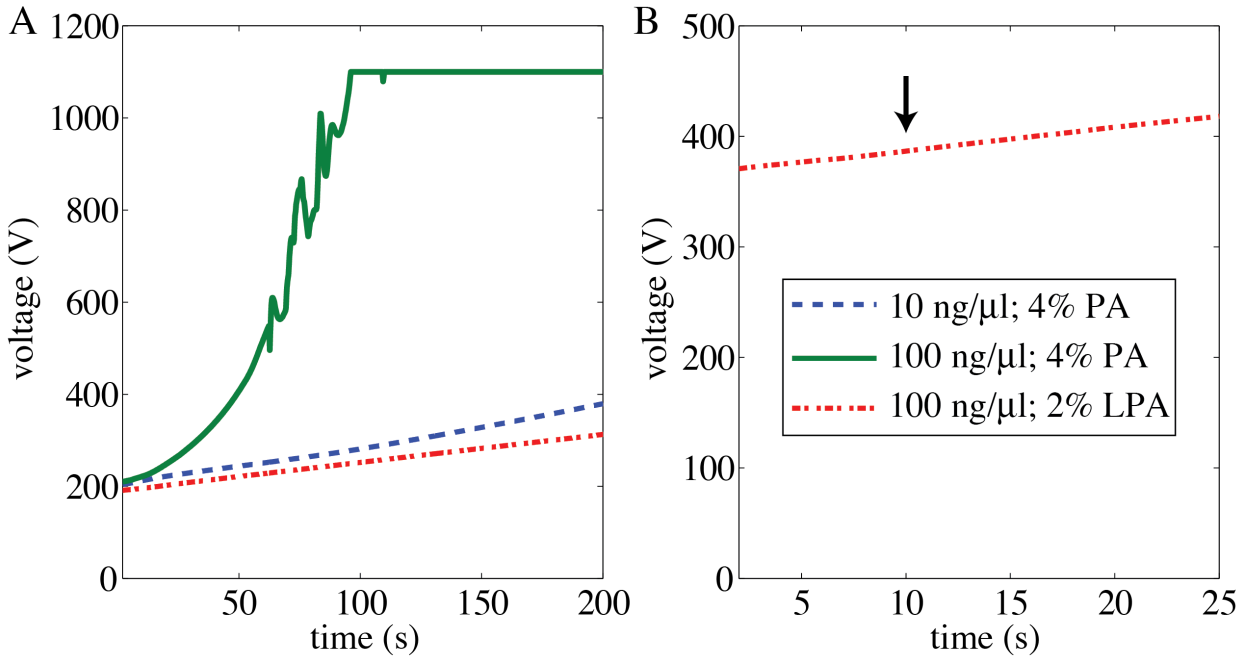

Figure S4. Experimental observation of voltage fluctuations caused by gel damage and elimination of these fluctuations by using a first-stage linear polymer injection region. (A) Voltage traces for total RNA injection experiments performed with 4% PA (blue nad green) and an initial 2% LPA region in series with 4% PA (red). For experiments with only 4% PA, we observed voltage fluctuations only for high concentration total RNA injections (100 ng/µl total RNA, shown in green). For experiments where we added a first-stage 2% LPA region, we did not observe voltage fluctuations when injecting 100 ng/µl total RNA. These data suggest that focused total RNAs can enter the 2% LPA withou causing degradation. (B) Later-time voltage trace during transition of the ITP interface from 2% LPA injection region to 4% PA. The transition occurs approximately where indicated by the arrow. We did not observe voltage fluctuations or gel degradation at this transition, suggesting that use of an initial-stage 2% LPA region succesfully prevents gel degradation.

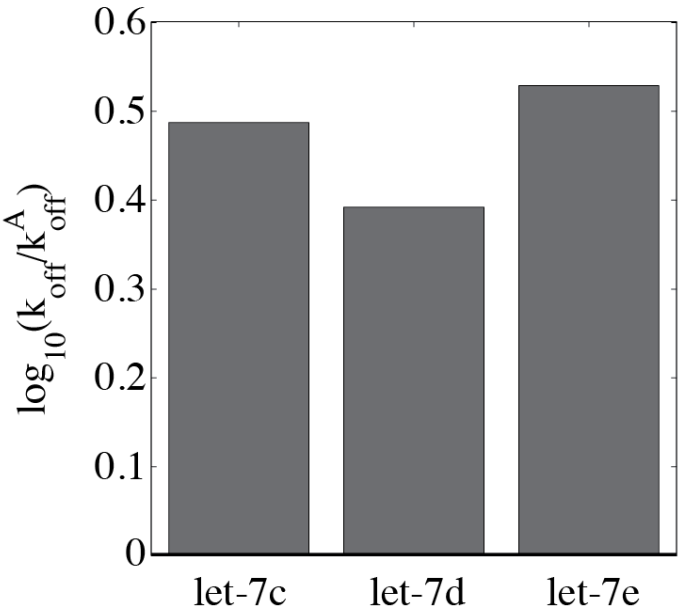

Figure S5. Estimate of relative kinetic off-rates for mismatch sequences. We measured the fluorescent signal for let-7a, two 1 nt mismatches (let-7c, let-7e), and one 2 nt mismatch (let-7d) at locations 1 cm and 2 cm along the channel measured from the start of the capture gel (LE3). We then estimated k_{off} using a simplified reaction rate equation (see text). Here we plot k_{off} for mismatch sequences relative to let-7a. As shown here, all mismatches have higher off-rates than let-7a. This suggests that off-rate kinetics play an important role in improving specificity of our assay.

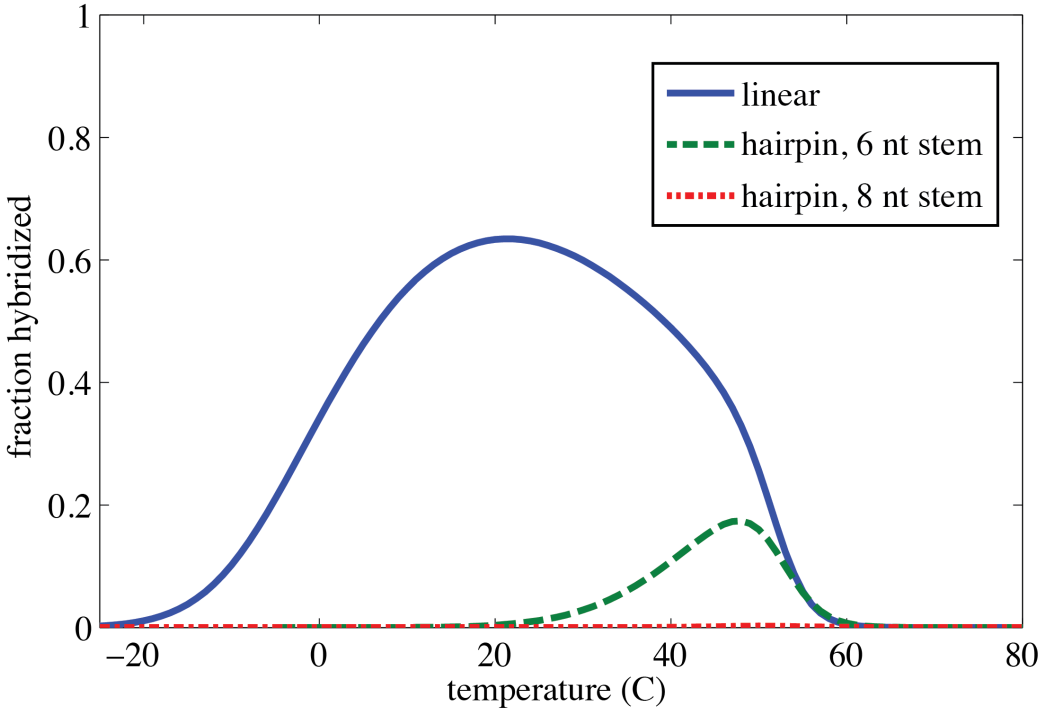

Figure S6. The effect of reporter secondary structure on equilibrium hybridization fraction to the let-7a precursor (pre-let-7a). We generated melting curves numerically for reactions between pre-let-7a and each of three reporter molecule designs: linear, hairpin with a 6nt stem, and hairpin with an 8nt stem. The linear reporter is fully-complementary to let-7a, while the hairpin reporters have a loop region which is complementary to let-7a and a stem region which is self-complementary. We observed that a linear design achieves a relatively high hybridized fraction. However, a hairpin design with a 6nt stem reduces this fraction significantly and a hairpin design with an 8nt stem completely eliminates hybridization with pre-let-7a. We use the hairpin reporter design with 8nt stem in all of our experiments.

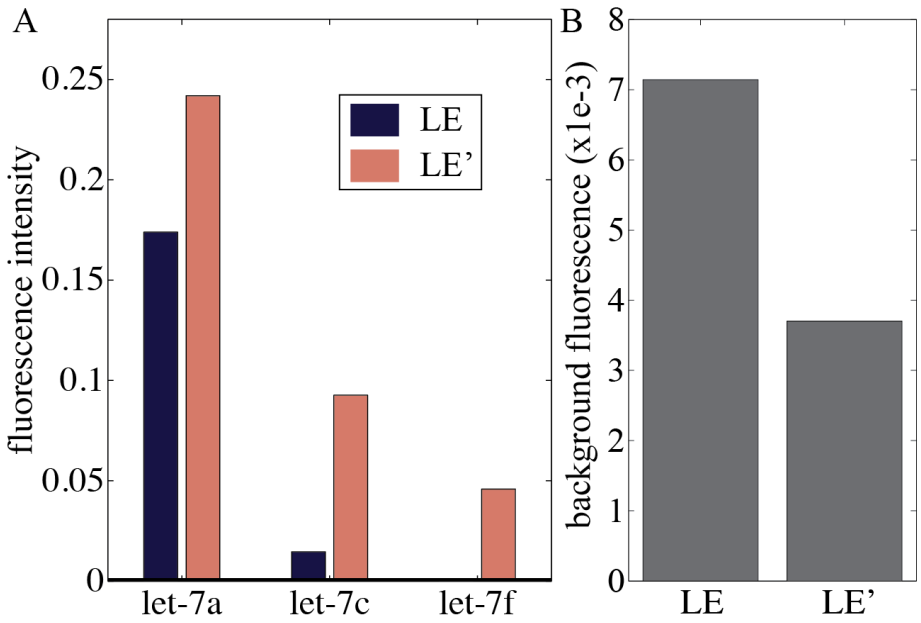

Figure S7. Experimental measurements demonstrating effect of magnesium on let-7a fluorescence signal, specificity, and affinity gel capture efficiency. We performed experiments using our buffer optimized for 1nt stringency (LE) and the same buffer with 1 mM magnesium chloride added (LE'). (A) We measured raw fluorescence signal for 500 pM let-7a, 7c, and 7f using both LE and LE'. We observe that adding magnesium improves let-7a signal by 41%, which in turn improves assay sensitivity. Non-specific let-7c and let-7f signals also increase, but remain lower than the let-7a signal. (B) We measured background fluorescent signal generated in a negative control experiment (no microRNA added). We see that LE' reduces background ~2-fold, thereby improving capture efficiency, assay dynamic range, and sensitivity.